

Research



Cite this article: Leandro J *et al.* 2022 Characterization and structure of the human lysine-2-oxoglutarate reductase domain, a novel therapeutic target for treatment of glutaric aciduria type 1. *Open Biol.* **12**: 220179. <https://doi.org/10.1098/rsob.220179>

Received: 7 June 2022

Accepted: 30 August 2022

Subject Area:

biochemistry/structural biology/cellular biology/developmental biology

Keywords:

crystal structure, glutaric aciduria, inborn errors of metabolism, lysine metabolism, enzymology, assay development

Authors for correspondence:

Sander M. Houten

e-mail: sander.houten@mssm.edu

Michael B. Lazarus

e-mail: michael.lazarus@mssm.edu

Electronic supplementary material is available online at <https://doi.org/10.6084/m9.figshare.c.6186147>.

Characterization and structure of the human lysine-2-oxoglutarate reductase domain, a novel therapeutic target for treatment of glutaric aciduria type 1

João Leandro¹, Susmita Khamrui^{2,3}, Chalada Suebsuwong^{2,3}, Peng-Jen Chen^{2,3}, Cody Secor^{2,3}, Tetyana Dodatko¹, Chunli Yu^{1,4}, Roberto Sanchez^{2,3}, Robert J. DeVita^{2,3}, Sander M. Houten¹ and Michael B. Lazarus^{2,3}

¹Department of Genetics and Genomic Sciences, ²Department of Pharmacological Sciences, and ³Drug Discovery Institute, Icahn School of Medicine at Mount Sinai, New York, NY 10029, USA

⁴Mount Sinai Genomics, Inc, Stamford, CT 06902, USA

SMH, 0000-0002-6167-9147; MBL, 0000-0002-6738-2563

In humans, a single enzyme 2-aminoadipic semialdehyde synthase (AASS) catalyses the initial two critical reactions in the lysine degradation pathway. This enzyme evolved to be a bifunctional enzyme with both lysine-2-oxoglutarate reductase (LOR) and saccharopine dehydrogenase domains (SDH). Moreover, AASS is a unique drug target for inborn errors of metabolism such as glutaric aciduria type 1 that arise from deficiencies downstream in the lysine degradation pathway. While work has been done to elucidate the SDH domain structurally and to develop inhibitors, neither has been done for the LOR domain. Here, we purify and characterize LOR and show that it is activated by alkylation of cysteine 414 by N-ethylmaleimide. We also provide evidence that AASS is rate-limiting upon high lysine exposure of mice. Finally, we present the crystal structure of the human LOR domain. Our combined work should enable future efforts to identify inhibitors of this novel drug target.

1. Introduction

The first step in lysine degradation via ϵ -deamination, also known as the saccharopine pathway, is catalysed by 2-aminoadipic acid semialdehyde synthase (AASS). AASS is a bifunctional enzyme with an N-terminal lysine-2-oxoglutarate reductase (LOR) domain and a C-terminal saccharopine dehydrogenase (SDH) domain (figure 1*a*), which are homologous to *Saccharomyces cerevisiae* LYS1 and LYS9, respectively [1]. The LOR domain catalyses the reductive deamination of L-lysine and 2-oxoglutarate into saccharopine (EC 1.5.1.8), which constitutes the first committed, and possibly rate-limiting, step in lysine degradation. SDH then oxidizes saccharopine into 2-aminoadipic semialdehyde and glutamate (EC 1.5.1.9). The bifunctional domain structure is conserved in all animals, but also *Dictyostelium discoideum* and plants, and seems to be associated with a function in lysine catabolism [2]. Fungi such as *S. cerevisiae* use the saccharopine pathway for lysine biosynthesis.

Several inborn errors of metabolism occur in the lysine degradation pathway. Hyperlysinemia caused by AASS deficiency due to mutations in AASS (MIM 238 700), is currently regarded as a biochemical phenotype of questionable clinical significance [3]. This means that hyperlysinemia can be diagnosed through biochemical and genetic methods but is considered not harmful to the affected individual [4–7]. By contrast, two other inborn errors of lysine degradation, glutaric aciduria type 1 (GA1) caused by mutations in *GCDH* (MIM 231 670)

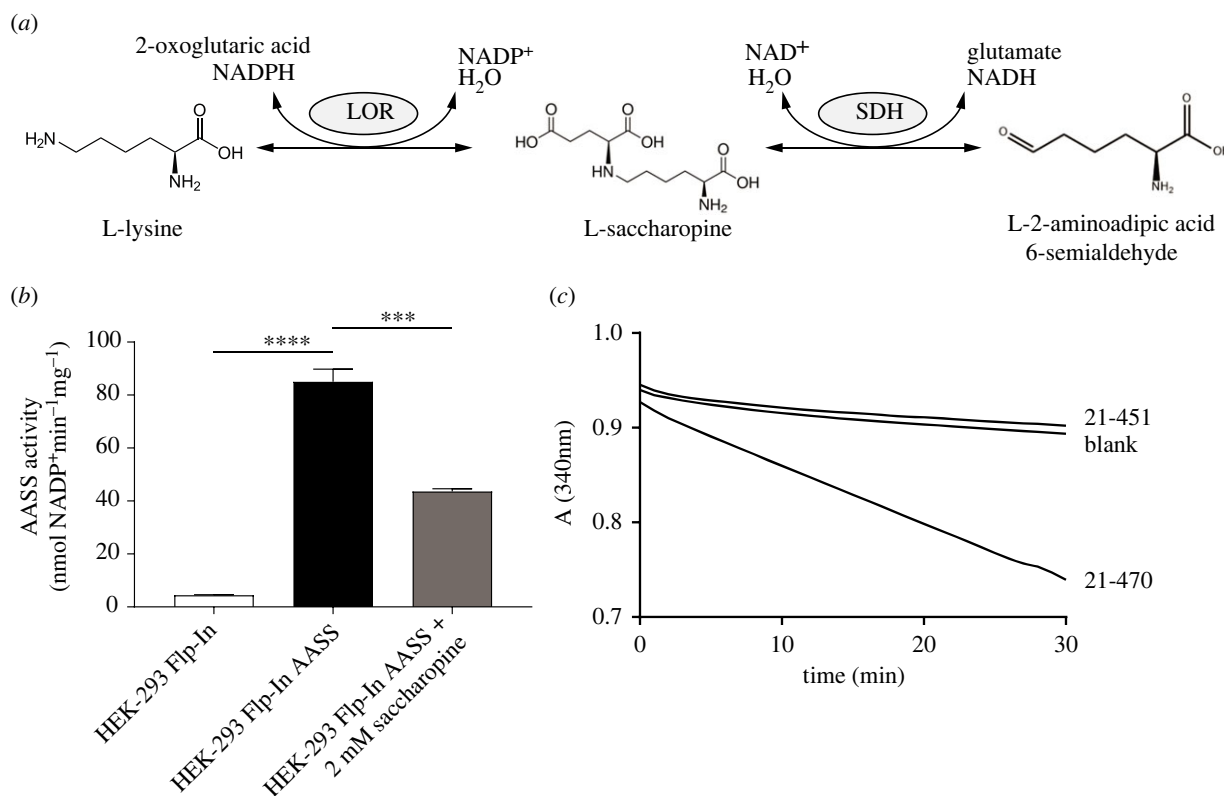


Figure 1. Characterization of AASS and the isolated LOR domain. (a) AASS reaction schema with the LOR and SDH activities. (b) Stable AASS expression in HEK-293 Flp-In cells and its inhibition by saccharopine. 10 mM 2-oxoglutarate (OG) was used as substrate. ***, $p < 0.001$; ****, $p < 0.0001$. Error bars indicate s.d. (c) Progress curves showing catalytic activity of a short (amino acids 21–451) and long LOR construct (amino acids 21–470), with 1 mM OG, measured in triplicate. Only the average absorption at 340 nm is displayed.

and pyridoxine-dependent epilepsy caused by mutations in *ALDH7A1* (PDE-ALDH7A1; MIM266 100), are serious diseases. These diseases are caused by toxicity of the accumulating substrates of the defective glutaryl-CoA dehydrogenase (GCDH) and antiquitin, respectively. Dietary intervention to decrease lysine intake is one part of the treatment for both disorders, which reduces lysine degradation pathway flux. Given that current treatment for these diseases is not optimal and that there is also an endogenous (non-dietary) source of lysine (i.e. through protein degradation), we and others have hypothesized that GA1 and PDE-ALDH7A1 can be treated by pharmacological substrate reduction therapy, through inhibition of AASS [8–10].

There is some debate on the contribution of AASS to the production of GCDH substrates in the brain [9–14]. However, recent studies including our own indicate that AASS is well expressed in human and mouse brain [9–12]. Importantly, we have shown that genetic inhibition of AASS was highly effective in limiting the accumulation of GCDH substrates in cell line and animal disease models of GA1 [10]. Although brain glutarate remained higher than in WT mice, the level in *Gcdh/Aass* double KO mice was 4-fold lower when compared to *Gcdh* single KO mice [10]. Since this therapeutic effect is comparable to the current treatment options, we believe AASS inhibition is a viable treatment strategy. Inhibition of the LOR domain is preferred given that it does not lead to accumulation of potentially toxic saccharopine [15–17].

Given the interest in AASS as a new therapeutic target for lysine metabolic disorders such as GA1, there is great need for small molecule inhibitors that provide pharmacological proof-of-concept for efficacy of this approach. However, two major bottlenecks to drug discovery for this project remained,

which are lack of a recombinant purification system and a high-resolution crystal structure of the enzyme. Resolving these would enable high throughput and virtual screening, respectively. Structures have been reported for the isolated human SDH domain (e.g. PDB code 5O1O) and for the *S. cerevisiae* LYS1, which has approximately 22% identity with the human LOR domain [18–20]. However, the low sequence identity of LYS1 diminishes its usefulness for drug discovery. Here, we describe enzyme and crystallographic studies including the first structure of the human LOR domain. We expect that these results will enable the future development of a high-affinity LOR inhibitor.

2. Results

2.1. Characterization of AASS-Myc-DDK and recombinant LOR enzymes

Pilot experiments aimed to overexpress AASS or its individual LOR and SDH domains in *Escherichia coli* indicated challenges in obtaining appreciable amounts of soluble protein. In order to characterize the protein, we initially transiently transfected HEK-293 cells with a plasmid encoding AASS with a C-terminal Myc-DDK tag (AASS-Myc-DDK) and used cell lysates as an enzyme source. Later, we generated and used Flp-In-293 cells stably overexpressing AASS-Myc-DDK. In both overexpression methods, LOR activity increased approximately 30-fold when compared to control lysates and was reliably determined using a spectrophotometric enzyme assay (figure 1b). LOR activity measured in the forward

Table 1. Steady-state kinetic properties of AASS-Myc-DDK and the LOR domain in forward and reverse reaction direction. The $K_{m, app}$ of partially purified AASS from human liver has been reported [21,22]. The pH optima in these studies were 7.8 for LOR forward and between pH 8.8 and 9.5 for LOR reverse. n is the Hill coefficient. ^aSubstrate inhibition. Values represent mean \pm s.d.

	purified human liver	AASS-Myc-DDK			isolated LOR		
	$K_{m, app}$ (mM)	$V_{max, app}$ (nmol min ⁻¹ mg ⁻¹)	$K_{m, app}$ (mM)	n	V_{max} (μ mol min ⁻¹ mg ⁻¹)	K_m (mM)	n
<i>forward direction</i>							
L-lysine	1.5	65 \pm 2	11 \pm 1	1.5 \pm 0.1	28.8 \pm 1.0	24 \pm 2	—
NADPH	1	273 \pm 99	0.42 \pm 0.02	1.8 \pm 0.1	65.4 \pm 2.7	0.39 \pm 0.02	2.1 \pm 0.2
2-oxoglutarate	0.08	106 \pm 5 ^a	1.2 \pm 0.1	1.5 \pm 0.1	57.2 \pm 1.0	1.4 \pm 0.1	—
<i>reverse direction</i>							
saccharopine	1.5	7.7 \pm 0.1	1.0 \pm 0.1	1.9 \pm 0.1	443 \pm 6	1.7 \pm 0.1	2.2 \pm 0.1
NADP ⁺	NR	7.4 \pm 0.4	1.0 \pm 0.1	-	525 \pm 5	0.42 \pm 0.01	1.6 \pm 0.1

direction was inhibited by saccharopine consistent with its ability to compete with lysine and 2-oxoglutarate [21].

The apparent steady-state kinetic properties of LOR in the full-length AASS-Myc-DDK were compared in the forward and reverse directions (table 1; electronic supplementary material, figure S1). The rate of the reverse reaction was considerably slower than that of the forward reaction, which is consistent with previous reports [23]. Positive cooperativity for several substrates is consistent with the reported tetrameric composition [23–25].

In order to optimize production of recombinant isolated LOR protein in *E. coli*, we evaluated several versions of His-tagged proteins for solubility and activity. We screened different length constructs in order to determine the appropriate domain boundaries. We were able to obtain large amounts of active soluble protein using an N-terminal His-sumo-tag construct with the mitochondrial transit peptide membrane segment removed (amino acids 21–470; figure 1c). This recombinant LOR was subsequently used to determine the steady-state kinetic properties. Overall, the kinetic constants resembled those of full-length AASS-Myc-DDK with the forward reaction velocity being considerably higher than the reverse (electronic supplementary material, figure S1; table 1).

2.2. AASS is activated by alkylation with N-ethylmaleimide

To explore if oxidation or reduction of cysteines could affect LOR activity, we evaluated tris(3-hydroxypropyl)phosphine (THP) and dithiothreitol (DTT) as reducing agents, and N-ethylmaleimide (NEM) as a sulfhydryl alkylating agent. Whereas DTT had no effect on LOR activity over a wide range of concentrations, THP inactivated the enzyme, but only at relatively high concentrations (greater than 250 μ M). Remarkably, NEM potentially activated LOR activity (figure 2a). The activation was not only concentration-dependent but also time-dependent, consistent with a covalent modification (figure 2b). At higher concentrations, the activating effect of NEM disappeared, but LOR activity stabilized at approximately 70% rather than showing complete inactivation. To demonstrate that the activation by NEM is also observed in full-length AASS, we tested NEM on LOR activity in lysates of Flp-In-293 cells

stably overexpressing AASS-Myc-DDK. In these cell lysates, LOR activity was also strongly activated by NEM in a concentration- and time-dependent manner comparable to the effects observed with isolated LOR (figure 2c).

To further establish that NEM activates LOR through alkylation, we first used OX-133, a monoclonal antibody recognizing NEM-modified cysteine residues in a sequence-independent manner [26]. Alkylation of LOR by NEM paralleled the activation pattern (figure 2d). Using X-ray crystallography (see below), we identified Cys 414 as alkylated by NEM. In order to establish if alkylation of Cys 414 is necessary for activation by NEM, we substituted this residue for alanine or glutamine. Both p.C414S and p.C414Q variants expressed and purified well. Both variants were not activated by NEM in contrast to the WT LOR (figure 2e). Specific activity of both variants was higher when compared to WT LOR. Further immunoblotting using the Cys 414 variants showed reduced, but not absent alkylation suggesting that at higher concentration of NEM other cysteines may also be modified, but are not needed for LOR activation (figure 2f).

2.3. AASS is rate-limiting *in vivo* upon high lysine exposure

If an enzyme is truly rate-limiting in a pathway, the concentration of the enzyme (i.e. expression level) determines flux. This can be evaluated by titrating the activity of an enzyme with a specific, irreversible inhibitor [27]. Such an inhibitor is currently not available for AASS. In order to start addressing the question whether AASS is rate-limiting *in vivo*, we used the *Aass* KO mouse model [10]. If AASS is a rate-limiting enzyme *in vivo*, *Aass*^{+/-} mice, which have a 50% reduction in AASS expression, should have decreased lysine degradation flux. We have previously measured key metabolites in a cohort of animals carrying *Gcdh* and *Aass* KO alleles on a chow diet [10]. We now grouped all mice according to their *Aass* genotype. As expected, *Aass* KO mice had elevated plasma lysine concentrations (figure 3). Plasma lysine in *Aass*^{+/-} mice was comparable to plasma lysine in *Aass*^{+/+} mice. This result argues against AASS catalysing the rate-limiting step in lysine catabolism under standard chow-fed conditions. We then exposed these mouse models to high

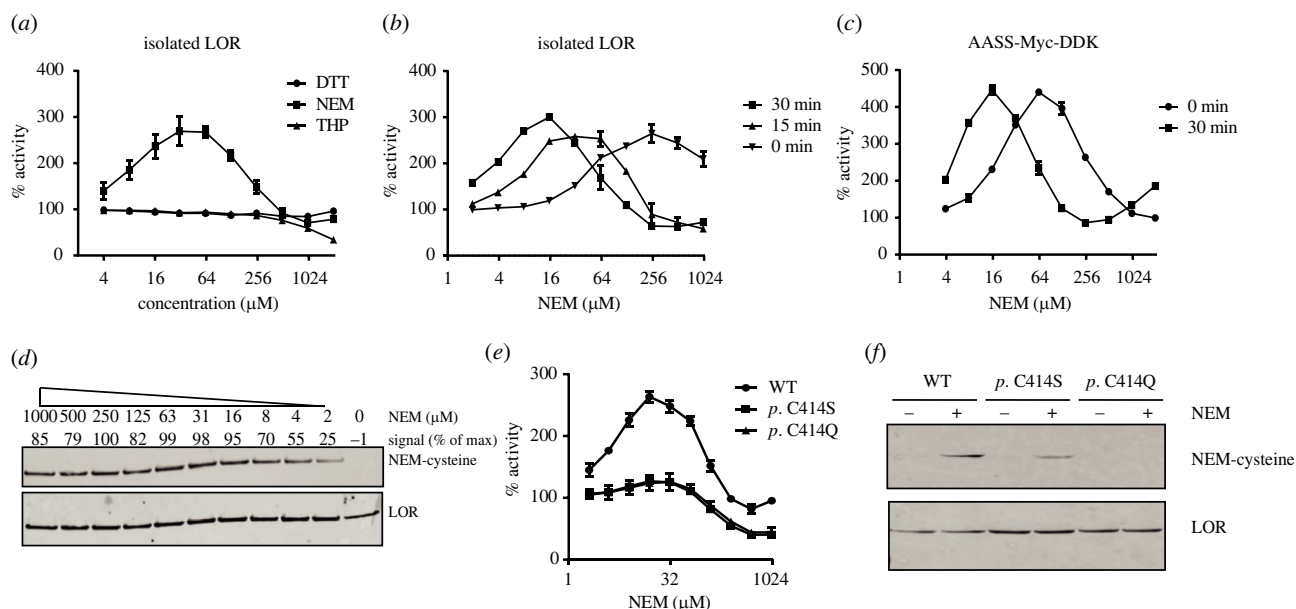


Figure 2. AASS activation by N-ethylmaleimide. (a) Effect of different concentrations of DTT ($n = 3$ for each concentration), THP ($n = 2$) and NEM ($n = 4$) on activity of the isolated LOR enzyme. (b) Time dependency of LOR activation by NEM. LOR was preincubated with the indicated concentration of NEM for 0, 15 or 30 min after which the reaction was started with 2-oxoglutarate. Each condition was tested in duplicate. (c) AASS-Myc-DDK activation by NEM. AASS-Myc-DDK was preincubated with the indicated concentration of NEM for 0 or 30 min after which the reaction was started with 2-oxoglutarate. Each condition was tested in triplicate. (d) Immunoblots of purified LOR treated for 10 minutes with the indicated concentration of NEM using anti-N-ethylmaleimide cysteine (OX-133) and anti-AASS antibodies. (e) Effect of different concentrations of NEM ($n = 4$) on activity of the isolated WT, p.C414S and p.C414Q LOR enzymes. (f) Immunoblots of purified WT, p.C414S and p.C414Q LOR enzymes treated for 10 minutes with 4 μ M of NEM using anti-N-ethylmaleimide cysteine (OX-133) and anti-His tag antibodies.

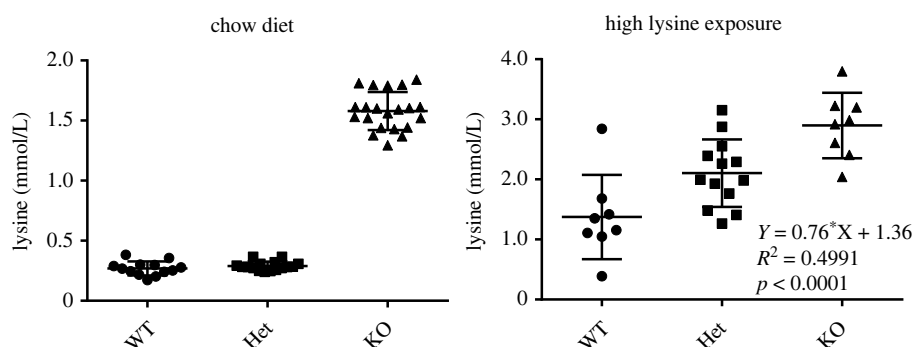


Figure 3. AASS is rate limiting upon high lysine exposure in mice. Plasma lysine concentration in mice on chow diet and upon high lysine exposure. Mice are grouped according to their genotype at the *Aass* locus (*Aass*^{+/+}, *Aass*^{+/-} and *Aass*^{-/-}). Each group contains *Gcdh*^{+/+}, *Gcdh*^{+/-} and *Gcdh*^{-/-} animals. Additional statistical analysis through a two-way ANOVA showed that the *Gcdh* locus did not explain variation in plasma lysine concentration (interaction: 4.79%, not significant; *Gcdh* genotype: 0.15%, not significant; and *Aass* genotype: 52.05%, $p = 0.0001$). A Tukey's multiple comparisons test shows significant differences between WT, Het and KO group (WT versus Het, $p < 0.05$; WT versus KO, $p < 0.001$; and Het versus KO, $p < 0.05$).

lysine through diet and drinking water. Under these conditions, the number of *Aass* KO alleles explains a significant percentage (50%) of the variation in plasma lysine concentrations with *Aass*^{+/-} animals clearly higher than those of *Aass*^{+/+} animals. Combined, these data suggest that AASS can be rate-limiting under conditions of high lysine load.

2.4. The crystal structure of the human LOR domain

No human structures have been reported for AASS/LOR, and the sequence identity with *S. cerevisiae* LYS1 is relatively low making structural prediction for the human enzyme challenging. We initially purified a short construct (amino acids 21–451) that expressed well in *E. coli* with high purity and a monodisperse peak on gel filtration. We screened conditions

and obtained crystals that after optimization diffracted to 2.2 Å and solved the structure (PDB 8E8T) by molecular replacement using the yeast LYS1 structure as a search model (electronic supplementary material, table S1). The overall structure of the human protein is quite similar to yeast LYS1 despite the low sequence identity, indicating strong conservation of function despite the evolved differences such as adopting bifunctional enzyme architecture and switching from NAD⁺ to NADP⁺. As seen in figure 4a, the LOR domain itself consists of two lobes, both Rossmann folds with a central beta-sheet with alpha helices on the outside. The lobes are connected twice with the C-terminus ending up in the N-terminal lobe. Some of the extended loops and predicted catalytic residues were not visible in this structure. Moreover, when we tested this short construct

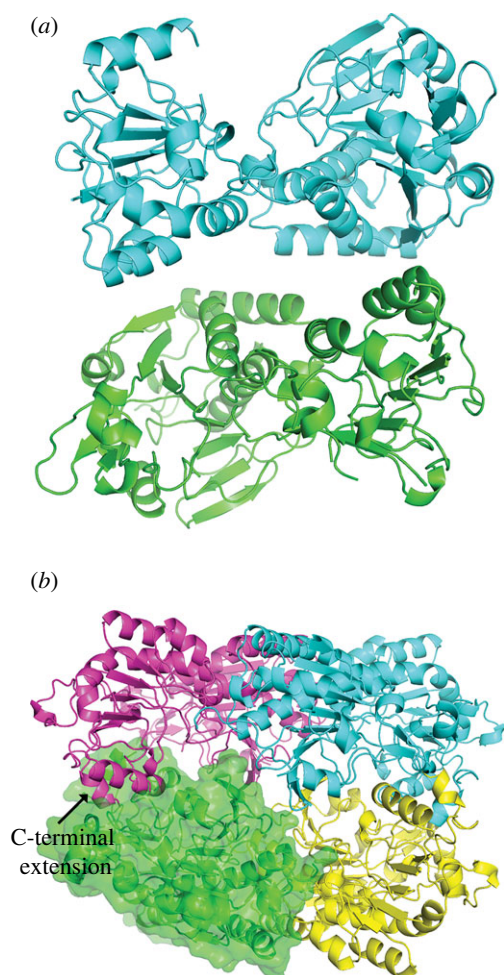


Figure 4. Overall structure of two LOR constructs. (a) Asymmetric unit of the short inactive construct shows a dimer of the LOR domain of AASS. The symmetry mate dimerization interface (electronic supplementary material, figure S3) is likely to be physiological. (b) Tetrameric structure of the long LOR constructs shown the four monomers assembling into a compact sphere. A surface is shown for one of the monomers to highlight the packing.

for activity, we discovered that, despite the fact that it was well folded and aligned nicely with the yeast structure, it had no activity in our *in vitro* assay (figure 1c).

Therefore, to obtain an LOR structure of a protein that maintained catalytic activity, we focused on the longer construct (amino acids 21–470). This initial construct crystallized readily but did not diffract well; therefore, we introduced five surface mutations to induce better packing. We were then able to obtain a crystal structure of the longer active construct, solving the structure (PDB 8E8U) by molecular replacement with the short construct. The longer construct crystallized in a new space group as a tetramer (figure 4b). Each monomer is very similar to the short construct with a root-mean-square deviation (RMSD) of 0.5691 \AA^2 between the most similar chains.

Several lines of evidence support an oligomeric state for AASS. Both constructs were eluted on gel filtration on a Superdex200 Increase column at around 12.5 ml, which equates to an approximate molecular weight between 150 and 200 kDa (electronic supplementary material, figure S2). This would suggest either a trimer or tetramer. Secondly, the dimeric interface is quite large. According to the PISA server, the average dimer interface of the longer construct is 1810 \AA^2 with a predicted ΔG of -6 kcal mol^{-1} . We reanalysed the structure of the short construct and noticed that although

the interface in the asymmetric unit is likely non-physiologic, the interface of a monomer with its crystallographic symmetry-mate is identical to the long interface in the tetramer (electronic supplementary material, figure S3), further supporting the validity of this interface. Next, the kinetic analysis of the recombinant LOR enzyme is also consistent with a multimer, given the cooperativity observed for NADP^+ (electronic supplementary material, figure S1).

At a structural level, the C-terminus of the longer construct forms an alpha helix that penetrates into the active site of the adjacent monomer. One paradox to resolve was why the C-terminus is so critical for activity, despite the fact that it is distant from the active site and the shorter construct is well folded. One hypothesis is that the C-terminus interacts with the catalytic residues of an adjacent monomer with the enzyme active only in an oligomeric state. Early on, it was reported in the literature that full-length human AASS exists as a tetramer when isolated from liver [24], consistent with our observations. Now, we have structural information on the tetrameric interface.

Compared to the yeast structure, the human one has two large insertions, both in the C-terminal lobe. First, there is a 37-amino acid insertion after residue 262. We see good density for this insertion, which forms two additional short alpha helices that extend away from the tetramer. The second is an insertion after residue 375, which forms a beta-sheet extension in the C-terminal lobe. In the structure of the long construct, we see electron density at the interface of these loops from two different monomers that sit between Asp 388 sidechains from each monomer and Glu 373 carbonyl backbones from each monomer (electronic supplementary material, figure S4). We have assigned this density to a magnesium ion which could help neutralize the negative charge from the aspartates. It is most likely to be hydrated given the distance between the aspartates, but we cannot see enough density for the water shell at the resolution of this structure.

Another important difference between LYS1 and LOR is that the human protein evolved to use NADPH while yeast uses NADH. This allows the LOR to drive the reaction toward production of saccharopine due to the much higher (essentially fully reduced) ratio of $\text{NADPH}/\text{NADP}^+$ compared to NADH/NAD^+ . Therefore, we would expect changes in the binding pocket to accommodate the phosphate group on NADP^+ . We were unable to obtain a crystal structure with substrates bound, presumably due to the low affinity to AASS for all of its substrates. However, the structure overlays favourably with the yeast structure bound to NAD^+ and therefore we can predict the key interactions. Initial alignments [19] predicted the human protein has glutamate where the yeast binds the ribose of NADH. However, in the structure we can see that the Ser 266 and Arg 267 sidechains match up to where the aspartate resides in the yeast structure (electronic supplementary material, figure S4). This explains why the human protein can bind the NADPH, replacing the negative charge of the yeast loop with a hydroxyl group (of Ser 266) and a positively charged Arg 267 to interact with the additional phosphate of NADPH.

We were also able to obtain a crystal structure of NEM-alkylated LOR short construct (PDB 8E8V). In the structure, there was unambiguous electron density for alkylation at only one position, Cys 414. We were able to model the NEM, which becomes N-ethylsuccinimide upon reaction with the cysteine, in the density and refine it with restraints for the

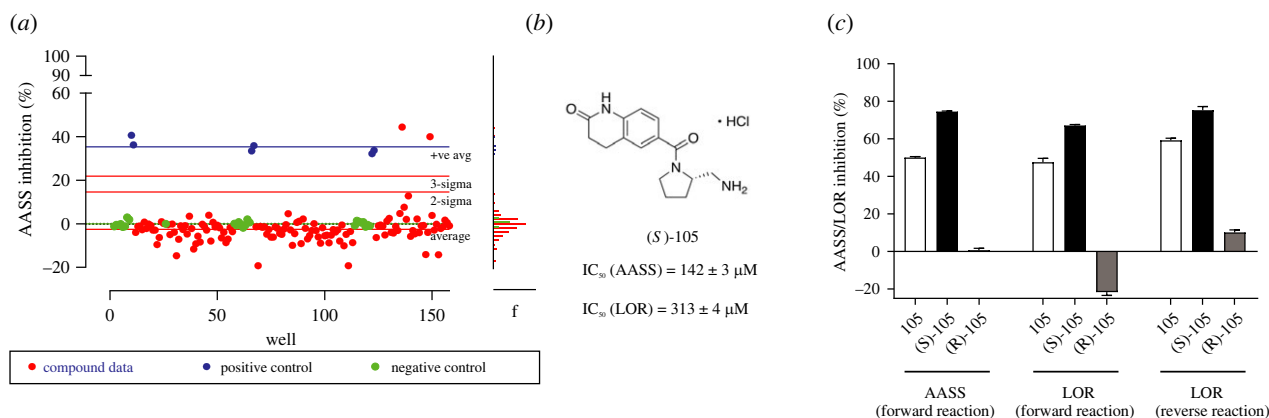


Figure 5. Development of an LOR assay to screen for inhibitors. (a) Signal to noise of assay shows good properties for a screen, with standard deviations indicated in red lines. The Z-factor is typically between 0.7 and 0.8. (b) Structure and IC_{50} of AASS/LOR inhibitor 105. (c) Full-length AASS inhibition in the forward reaction and LOR domain inhibition in the forward and reverse reaction by inhibitor 105 and its stereoisomers at a concentration of 300 μ M. 1 mM 2-oxoglutarate was used as a substrate.

sulfur-carbon bond. Subsequently, we were able to identify biochemically that Cys 414 is a key residue in the activation of LOR (figure 2e). Interestingly, there are no obvious other differences between the apo and NEM structures. However, Cys 414 sits at the interface of the two lobes of the LOR, suggesting it is an important location for regulating activity (electronic supplementary material, figure S5).

2.5. Amino acid substitutions causing AASS deficiency and hyperlysinemia

Hyperlysinemia in humans has been associated with the p.R65Q, p.A154T and p.L419R variants in the LOR domain of AASS [4]. Our earlier work showed that many of these mutations lead to loss of protein expression [4] and with our structure, we can better understand the consequences of these amino acid substitutions on the LOR structure. Arg 65 makes several important contacts including a salt bridge to Asp 69 and a hydrogen bonding interaction with the carbonyl backbone of Gln 60, helping to stabilize several portions of the N-lobe. Ala 154 is located exactly where the nicotinamide moiety of NAD^+ binds in the yeast structure, so the threonine would likely preclude its binding. The Alanine-Glycine motif from 154–155 is conserved from the yeast protein to the human one, likely because any larger sidechains would obstruct nicotinamide binding. Lastly, Leu 419 is buried in a hydrophobic pocket in the N-lobe, so an arginine sidechain would probably destabilize the pocket.

2.6. Development and validation of a LOR assay suitable for high throughput screening

Since AASS is a viable therapeutic target for GA1, our next objective was to further develop and validate an assay amenable to high throughput screening for identifying inhibitors of the LOR domain. We used the absorption at 340 nm to monitor NADPH consumption in a 96-well plate format. In order to identify compounds to help validate the assay, we performed a virtual screen to identify potential active site inhibitors to assess viability of the assay. We purchased 126 commercially available potential hit compounds identified by virtual screen (electronic supplementary material,

table S2A), then tested them in the LOR enzyme assay. As seen in figure 5a, almost all compounds had minimal effect on activity. However, we identified one compound, 105, that showed inhibition several standard deviations away from the average. We then re-synthesized racemic compound 105, which contains one chiral center (figure 5b) to confirm its activity. We also prepared both 105 enantiomers found that only the S-105 enantiomer was active against both the recombinant LOR protein and the full-length AASS construct (figure 5c). Additional purchased and synthesized compounds did not show improved potency (electronic supplementary material, table S2B,C and figures S6–S8). However, while the potency of this compound was modest, it demonstrated that the assay was robust, dose responsive and useful to identify inhibitors. There is also the possibility to further miniaturize to a 384-well plate format with incubation at room temperature for high-throughput screens. We expect these results to enable discovery of more potent inhibitors of LOR using an *unbiased* large library screen for identification of both active or allosteric site inhibitors.

3. Discussion

AASS is an important enzyme in lysine degradation and a potentially attractive pharmacological target for the treatment of two inborn errors of metabolism, GA1 and PDE-ALDH7A1. Herein, we developed chemical and biological tools that can be useful for the future development of a high affinity inhibitor of the LOR domain of AASS. We over-expressed AASS-Myc-DDK, purified a recombinant isolated LOR domain, and determined the kinetic constants of these enzymes. We used this knowledge to develop an LOR enzyme assay amenable to high throughput screening for inhibitors. The LOR assay was validated in a virtual screen that identified one compound with modest inhibition activity (IC_{50} 142 μ M). Importantly, we solved the first crystal structure of the human LOR domain at 2.2 Å resolution.

AASS catalyses the first committed, and possibly rate-limiting, step in lysine degradation. Although the LOR reaction is reversible *in vitro*, *in vivo* it is likely driven toward the production of saccharopine by the nearly fully reduced NADPH/NADP⁺ ratio in mitochondria. A defect in the mitochondrial biosynthesis of NADP⁺ leads to hyperlysinemia

demonstrating that in man and mouse NADPH cannot be replaced by NADH [28–31]. There is evidence that limited 2-oxoglutarate availability in some inborn errors of metabolism, such as urea cycle defects, limits lysine degradation [32], but it is unknown if 2-oxoglutarate is limiting under non-pathological conditions. The affinity of AASS for lysine is relatively low. The previously reported K_m of partially purified AASS/LOR from human liver was 1.5 mM [21] (table 1). We calculated a K_m of 11 mM for AASS-Myc-DDK and 24 mM for isolated LOR. Plasma concentrations of lysine are usually lower than 300 $\mu\text{mol l}^{-1}$ [4,10]. Estimated tissue concentrations for lysine are very similar (336 $\mu\text{mol l}^{-1}$ for liver and 142 $\mu\text{mol l}^{-1}$ for heart based on reference [33]). The low affinity of AASS/LOR for lysine in combination with the estimated tissue lysine concentration suggests that the velocity of lysine degradation will show a linear relationship to the mitochondrial lysine concentration. However, a gene-dose effect on plasma lysine concentration in mice carrying one *Aass* null allele was only observed upon high lysine exposure. No such effect was evident in mice on chow diet, which likely supplies lysine in quantities close to the actual nutritional requirement. Therefore, we speculate that with a relatively low, but adequate lysine supply, the rate of its degradation is determined by cellular lysine uptake and subsequent protein synthesis and not by AASS activity. Although there is little available information on lysine transport across the plasma and mitochondrial membrane, it is likely driven by lysine concentration in a saturable process [34,35]. By contrast, under conditions with a larger supply of lysine, for example, during catabolism or postprandial, AASS/LOR catalyses the rate-limiting step in lysine degradation and thus reinforces the notion that inhibiting of LOR is a suitable strategy in the treatment of GA1.

It has been reported that during acute illness the urinary excretion of glutaric and 3-hydroxyglutaric acid can rise dramatically with values 4-fold higher than observed as compared to baseline illness [36]. Such changes in lysine degradation flux suggest the potential of allosteric activation of AASS. We provide evidence that AASS can be activated *in vitro* by alkylation of Cys 414 using NEM. This modification suggests a novel site of allosteric activation of the enzyme, although the mechanism is still unknown. Allosteric activation is a common feature in many metabolic pathways. For example, the human glycolysis enzyme pyruvate kinase M2 (PKM2) is activated by fructose 1,6-bisphosphate and certain amino acids, which promotes tetramerization of the enzyme [37]. Another example is glutamate dehydrogenase (GDH), which is activated by ADP and leucine and inhibited by GTP, palmitoyl-CoA and ATP [38]. In addition, GDH is inhibited by binding to short-chain 3-hydroxyacyl-CoA dehydrogenase [39]. Thus, there are diverse and complex mechanisms of allosteric regulation for many metabolic enzymes. Future work identifying the mechanism of activation will help shed light on lysine metabolism regulation and may provide additional insights onto substrate reduction strategies for GA1.

To conclude, we have characterized and purified the LOR domain of the important metabolic enzyme AASS. We show that AASS can be rate-limiting in the pathway and present the first crystal structure of the human LOR domain. We established an assay to measure inhibition of AASS in high throughput and identified a weak inhibitor by virtual screen that helped validate our assay. The development of a recombinant purification system and a high-resolution crystal structure and will enable future efforts to further validate this enzyme as a potential therapeutic target for the treatment of GA1 and will enable improved inhibitor discovery to provide pharmacological proof of concept for efficacy in cells and *in vivo*.

Data accessibility. Coordinates and structure factors for the crystal structures have been deposited to the PDB.

Additional supporting data and a complete description of the methods are provided in electronic supplementary material [40].

Authors' contributions. J.L.: conceptualization, data curation, formal analysis, investigation, methodology, writing—review and editing; S.K.: conceptualization, data curation, formal analysis, investigation, methodology; C.Su.: conceptualization, data curation, formal analysis, investigation, methodology; P.-J.C.: conceptualization, data curation, formal analysis, investigation, methodology; C.Se.: data curation, investigation, methodology; T.D.: conceptualization, data curation, formal analysis, investigation, methodology; C.Y.: conceptualization, data curation, formal analysis, investigation, methodology, project administration; R.S.: conceptualization, data curation, formal analysis, investigation, methodology, project administration, writing—review and editing; R.J.D.: conceptualization, data curation, formal analysis, funding acquisition, investigation, methodology, project administration, writing—review and editing; S.M.H.: conceptualization, data curation, formal analysis, funding acquisition, investigation, methodology, project administration, supervision, writing—original draft, writing—review and editing; M.B.L.: conceptualization, data curation, formal analysis, funding acquisition, investigation, methodology, project administration, supervision, writing—original draft, writing—review and editing.

All authors gave final approval for publication and agreed to be held accountable for the work performed therein.

Conflict of interest declaration. The authors declare no competing interests.

Funding. Research reported in this publication was supported by the Eunice Kennedy Shriver National Institute of Child Health & Human Development and the National Institute of General Medical Sciences of the National Institutes of Health under Award Numbers R21HD102745 (to S.M.H. and R.J.D.) and R35GM124838 (to M.B.L.). This research used resources of the National Synchrotron Light Source II, a US Department of Energy (DOE) Office of Science User Facility operated for the DOE Office of Science by Brookhaven National Laboratory, under Contract No. DESC0012704. The Life Science Biomedical Technology Research resource is primarily supported by the NIH, National Institute of General Medical Sciences (NIGMS) through a Biomedical Technology Research Resource P41 grant (No. P41GM111244), and by the DOE Office of Biological and Environmental Research (No. KP1605010). This work used the NMR Spectrometer Systems at Mount Sinai acquired with funding from National Institutes of Health SIG grants 1S10OD025132 and 1S10OD028504.

Acknowledgements. The content is solely the responsibility of the authors and does not necessarily represent the official views of the National Institutes of Health.

References

1. Sacksteder KA, Biery BJ, Morrell JC, Goodman BK, Geisbrecht BV, Cox RP, Gould SJ, Geraghty MT. 2000 Identification of the alpha-amino adipic semialdehyde synthase gene, which is defective in familial hyperlysinemia. *Am. J. Hum. Genet.* **66**, 1736–1743. (doi:10.1086/302919)
2. Serrano GC, Rezende e Silva Figueira T, Kiyota E, Zanata N, Arruda P. 2012 Lysine degradation through the saccharopine pathway in bacteria: LKR and SDH in bacteria and its relationship to the plant and animal enzymes. *FEBS Lett.* **586**, 905–911. (doi:10.1016/j.febslet.2012.02.023)

3. Goodman SI, Duran M. 2014 Biochemical phenotypes of questionable clinical significance. In *Physician's guide to the diagnosis, treatment, and follow-up of inherited metabolic diseases* (eds N Blau, M Duran, KM Gibson, C Dionisi-Vici), pp. 691–705. Berlin, Germany: Springer Verlag.
4. Houten SM *et al.* 2013 Genetic basis of hyperlysinemia. *Orphanet J. Rare Dis.* **8**, 57. (doi:10.1186/1750-1172-8-57)
5. Gregory JW, Beail N, Boyle NA, Dobrowski C, Jackson P. 1989 Dietary treatment of hyperlysinemia. *Arch. Dis. Child* **64**, 716–720. (doi:10.1136/adc.64.5.716)
6. van der Heiden C, Brink M, de Bree PK, van Sprang FJ, Wadman SK, de Pater JM, van Biervliet JP. 1978 Familial hyperlysinemia due to L-lysine alpha-ketoglutarate reductase deficiency: results of attempted treatment. *J. Inher. Metab. Dis.* **1**, 89–94. (doi:10.1007/BF01805679)
7. Dancis J, Hutzler J, Ampola MG, Shih VE, van Gelderen HH, Kirby LT, Woody NC. 1983 The prognosis of hyperlysinemia: an interim report. *Am. J. Hum. Genet.* **35**, 438–442.
8. Pena IA, MacKenzie A, Van Karnebeek CDM. 2017 Current knowledge for pyridoxine-dependent epilepsy: a 2016 update. *Expert Rev. Endocrinol. Metab.* **12**, 5–20. (doi:10.1080/17446651.2017.1273107)
9. Pena IA, Marques LA, Laranjeira AB, Yunes JA, Eberlin MN, MacKenzie A, Arruda P. 2017 Mouse lysine catabolism to amino adipate occurs primarily through the saccharopine pathway; implications for pyridoxine dependent epilepsy (PDE). *Biochim. Biophys. Acta* **1863**, 121–128. (doi:10.1016/j.bbadis.2016.09.006)
10. Leandro J, Dodatko T, DeVita RJ, Chen H, Stauffer B, Yu C, Houten SM. 2020 Deletion of 2-amino adipic semialdehyde synthase limits metabolite accumulation in cell and mouse models for glutaric aciduria type 1. *J. Inher. Metab. Dis.* **43**, 1154–1164. (doi:10.1002/jimd.12276)
11. Crowther LM, Mathis D, Poms M, Plecko B. 2019 New insights into human lysine degradation pathways with relevance to pyridoxine dependent epilepsy due to antiquitin deficiency. *J. Inher. Metab. Dis.* **42**, 620–628. (doi:10.1002/jimd.12076)
12. Posset R, Opp S, Struys EA, Volkl A, Mohr H, Hoffmann GF, Kölker S, Sauer SW, Okun JG. 2015 Understanding cerebral L-lysine metabolism: the role of L-pipecolate metabolism in Gcdh-deficient mice as a model for glutaric aciduria type I. *J. Inher. Metab. Dis.* **38**, 265–272. (doi:10.1007/s10545-014-9762-z)
13. Hallen A, Jamie JF, Cooper AJ. 2013 Lysine metabolism in mammalian brain: an update on the importance of recent discoveries. *Amino Acids* **45**, 1249–1272. (doi:10.1007/s00726-013-1590-1)
14. Sauer SW, Opp S, Hoffmann GF, Koeller DM, Okun JG, Kölker S. 2011 Therapeutic modulation of cerebral L-lysine metabolism in a mouse model for glutaric aciduria type I. *Brain* **134**, 157–170. (doi:10.1093/brain/awq269)
15. Guo Y, Wu J, Wang M, Wang X, Jian Y, Yang C, Guo W. 2022 The metabolite saccharopine impairs neuronal development by inhibiting the neurotrophic function of glucose-6-phosphate isomerase. *J. Neurosci.* **42**, 2631–2646. (doi:10.1523/JNEUROSCI.1459-21.2022)
16. Zhou J *et al.* 2019 The lysine catabolite saccharopine impairs development by disrupting mitochondrial homeostasis. *J. Cell Biol.* **218**, 580–597. (doi:10.1083/jcb.201807204)
17. Leandro J, Houten SM. 2019 Saccharopine, a lysine degradation intermediate, is a mitochondrial toxin. *J. Cell Biol.* **218**, 391–392. (doi:10.1083/jcb.201901033)
18. Kumar VP, Thomas LM, Bobyk KD, Andi B, Cook PF, West AH. 2012 Evidence in support of lysine 77 and histidine 96 as acid-base catalytic residues in saccharopine dehydrogenase from *Saccharomyces cerevisiae*. *Biochemistry* **51**, 857–866. (doi:10.1021/bi201808u)
19. Burk DL, Hwang J, Kwok E, Marrone L, Goodfellow V, Dmitrienko GI, Berghuis AM. 2007 Structural studies of the final enzyme in the alpha-amino adipate pathway—saccharopine dehydrogenase from *Saccharomyces cerevisiae*. *J. Mol. Biol.* **373**, 745–754. (doi:10.1016/j.jmb.2007.08.044)
20. Andi B, Xu H, Cook PF, West AH. 2007 Crystal structures of ligand-bound saccharopine dehydrogenase from *Saccharomyces cerevisiae*. *Biochemistry* **46**, 12 512–12 521. (doi:10.1021/bi701428m)
21. Hutzler J, Dancis J. 1975 Lysine-ketoglutarate reductase in human tissues. *Biochim. Biophys. Acta* **377**, 42–51. (doi:10.1016/0005-2744(75)90284-3)
22. Dancis J, Hutzler J, Cox RP. 1979 Familial hyperlysinemia: enzyme studies, diagnostic methods, comments on terminology. *Am. J. Hum. Genet.* **31**, 290–299.
23. Noda C, Ichihara A. 1978 Purification and properties of L-lysine-alpha-ketoglutarate reductase from rat liver mitochondria. *Biochim. Biophys. Acta* **525**, 307–313. (doi:10.1016/0005-2744(78)90225-5)
24. Markovitz PJ, Chuang DT. 1987 The bifunctional amino adipic semialdehyde synthase in lysine degradation. Separation of reductase and dehydrogenase domains by limited proteolysis and column chromatography. *J. Biol. Chem.* **262**, 9353–9358. (doi:10.1016/S0021-9258(18)48087-8)
25. Markovitz PJ, Chuang DT, Cox RP. 1984 Familial hyperlysinemias. Purification and characterization of the bifunctional amino adipic semialdehyde synthase with lysine-ketoglutarate reductase and saccharopine dehydrogenase activities. *J. Biol. Chem.* **259**, 11 643–11 646. (doi:10.1016/S0021-9258(20)71252-4)
26. Holbrook LM, Kwong LS, Metcalfe CL, Fenouillet E, Jones IM, Barclay AN. 2016 OX133, a monoclonal antibody recognizing protein-bound N-ethylmaleimide for the identification of reduced disulfide bonds in proteins. *MAbs* **8**, 672–677. (doi:10.1080/19420862.2016.1152443)
27. Drynan L, Quant PA, Zammit VA. 1996 Flux control exerted by mitochondrial outer membrane carnitine palmitoyltransferase over beta-oxidation, ketogenesis and tricarboxylic acid cycle activity in hepatocytes isolated from rats in different metabolic states. *Biochem. J.* **317**(Pt 3), 791–795. (doi:10.1042/bj3170791)
28. Pomerantz DJ *et al.* 2018 Clinical heterogeneity of mitochondrial NAD kinase deficiency caused by a NADK2 start loss variant. *Am. J. Med. Genet. A* **176**, 692–698. (doi:10.1002/ajmg.a.38602)
29. Zhang K *et al.* 2018 Deficiency of the mitochondrial NAD kinase causes stress-induced hepatic steatosis in mice. *Gastroenterology* **154**, 224–237. (doi:10.1053/j.gastro.2017.09.010)
30. Tort F, Ugarteburu O, Torres MA, Garcia-Villoria J, Giros M, Ruiz A, Ribes A. 2016 Lysine restriction and pyridoxal phosphate administration in a NADK2 patient. *Pediatrics* **138**, e20154534. (doi:10.1542/peds.2015-4534)
31. Houten SM *et al.* 2014 Mitochondrial NAD(P)H deficiency due to a mutation in NADK2 causes dienoyl-CoA reductase deficiency with hyperlysinemia. *Hum. Mol. Genet.* **23**, 5009–5016. (doi:10.1093/hmg/ddu218)
32. Kamoun P, Richard V, Rabier D, Saudubray JM. 2002 Plasma lysine concentration and availability of 2-ketoglutarate in liver mitochondria. *J. Inher. Metab. Dis.* **25**, 1–6. (doi:10.1023/A:1015195009330)
33. Houten SM *et al.* 2013 Impaired amino acid metabolism contributes to fasting-induced hypoglycemia in fatty acid oxidation defects. *Hum. Mol. Genet.* **22**, 5249–5261. (doi:10.1093/hmg/ddt382)
34. Li X, Hui S, Mirek ET, Jonsson WO, Anthony TG, Lee WD, Zeng X, Jang C, Rabinowitz JD. 2022 Circulating metabolite homeostasis achieved through mass action. *Nat. Metab.* **4**, 141–152. (doi:10.1038/s42255-021-00517-1)
35. Ferruzza S, Ranaldi G, Di Girolamo M, Sambuy Y. 1995 The transport of lysine across monolayers of human cultured intestinal cells (Caco-2) depends on Na(+)-dependent and Na(+)-independent mechanisms on different plasma membrane domains. *J. Nutr.* **125**, 2577–2585.
36. Whelan DT, Hill R, Ryan ED, Spate M. 1979 L-Glutaric acidemia: investigation of a patient and his family. *Pediatrics* **63**, 88–93. (doi:10.1542/peds.63.1.88)
37. Akhtar K, Gupta V, Koul A, Alam N, Bhat R, Bamezai RN. 2009 Differential behavior of missense mutations in the intersubunit contact domain of the human pyruvate kinase M2 isozyme. *J. Biol. Chem.* **284**, 11 971–11 981. (doi:10.1074/jbc.M808761200)
38. Li M, Li C, Allen A, Stanley CA, Smith TJ. 2014 Glutamate dehydrogenase: structure, allosteric regulation, and role in insulin homeostasis. *Neurochem. Res.* **39**, 433–445. (doi:10.1007/s11064-013-1173-2)

39. Li C *et al.* 2010 Mechanism of hyperinsulinism in short-chain 3-hydroxyacyl-CoA dehydrogenase deficiency involves activation of glutamate dehydrogenase. *J. Biol. Chem.* **285**, 31 806–31 818. (doi:10.1074/jbc.M110.123638)
40. Leandro J *et al.* 2022 Data from: Characterization and structure of the human lysine-2-oxoglutarate reductase domain, a novel therapeutic target for treatment of glutaric aciduria type 1. Figshare. (doi:10.6084/m9.figshare.c.6186147)